Available online at www.sciencedirect.com
SCIENCE DIRECT®
Computers and Structures 82 (2004) 1033–1052
Computers & Structures
www.elsevier.com/locate/compstruc

Fuzzy reliability analysis of concrete structures

Fabio Biondini [a,*], Franco Bontempi [b], Pier Giorgio Malerba [a]

[a] Department of Structural Engineering, Technical University of Milan, P.za L. da Vinci, 32, Milan 20133, Italy
[b] Department of Structural and Geotechnical Engineering, University of Rome "La Sapienza", Italy

Accepted 5 March 2004

Abstract

This paper presents a methodological approach of wide generality for assessing the reliability of reinforced and prestressed concrete structures. As known, the numerical values of the parameters which define the geometrical and mechanical properties of this kind of structures, are affected by several sources of uncertainties. In a realistic approach such properties cannot be considered as deterministic quantities. In the present study all these uncertainties are modeled using a fuzzy criterion in which the model is not defined through a set of fixed values, but through bands of values, bounded between suitable minimum and maximum extremes. The reliability problem is formulated at the load level, with reference to several serviceability and ultimate limit states. For the critical interval associated to each limit state, the membership function of the safety factor is derived by solving a corresponding anti-optimization problem. The strategic planning of this solution process is governed by a genetic algorithm, which generates the sampling values of the parameters involved in the material and geometrical non-linear structural analyses. The effectiveness of the proposed approach and its capability to handle complex structural systems are shown by carrying out a reliability assessment of a prestressed concrete continuous beam and of a cable-stayed bridge.

Keywords: Structural reliability; Concrete structures; Non-linear analysis; Uncertainty; Fuzzy criteria; Anti-optimization; Genetic algorithms

1. Introduction

From the engineering point of view, a structural problem can be considered as "uncertain" when some lack of knowledge exists about the theoretical model which describes the structural system and its behavior, either with respect to the model itself, or to the value of its significant parameters. The uncertainty which affects the model, or a part of it, could be avoided through direct tests. Such process is typical, for example, of aeronautical and mechanical engineering, where tests on prototypes are performed before the series production and contribute to improve and to validate the model. In civil engineering the realization of structural prototypes is very unusual, not only for economical reasons, but also because a prototype tested in a laboratory can never fully represent the actual structure built on site.

To overcome such uncertainties, structural engineers always based their choices on the experience accumulated in the course of time. The same experience also allowed them to draw generalizations. However, difficulties arise when designers need to transfer the experience of the past to nowadays problems, where both the design choices and the nature itself of the structures are different. In this sense, particular attention must also be paid to special structures which cannot be listed in the traditional building categories and, as such, are not part of the experience inheritance from the past. In addition, due in particular to the growing complexity of structural systems faced by nowadays designers, the uncertain parameters involved in design evaluations tend to be

* Corresponding author. Tel.: +39-02-2399-4394; fax: +39-02-2399-4220.
E-mail address: biondini@stru.polimi.it (F. Biondini).

0045-7949/$ - see front matter © 2004 Elsevier Ltd. All rights reserved.
doi:10.1016/j.compstruc.2004.03.011

very numerous and highly interacting. As a consequence, a complete understanding of the sensitivity of the structural behavior with respect to such uncertainties is usually quite hard, and specific mathematical concepts and numerical methods are required for a reliable assessment of the structural safety [5].

Reliability-based concepts are nowadays widely accepted in structural design, even if it is well known that, before such concepts can be effectively implemented, the actual design problem often needs to be considerably simplified. This is mainly due to the two following reasons:

(1) In their simplest formulation, reliability-based procedures require the structural performance to be represented by explicit functional relationships among the load and the resistance variables. But, unfortunately, when the structural behavior is affected by several sources of non-linearity, as always happens for concrete structures, such relationships are generally available only in an implicit form.
(2) For structural systems with several components, a complete reliability analysis includes both component-level and system-level estimates. Depending on the number and on the arrangement of the components, system reliability evaluations can become very complicated and even practically impossible for large structural systems.

This paper proposes a theoretical approach and numerical procedures for the reliability assessment of reinforced and prestressed concrete structures, based on detailed and representative mechanical models, and able to handle implicit formulation of the performance relationships and to perform system-level evaluations even for large structural systems [3,4,9].

The uncertainties regarding the geometrical and mechanical properties involved in the structural problem, can be approached by a probabilistic or by a fuzzy formulation.

The probabilistic approach assumes the intrinsic stochastic variability of the random variables as known. In the practice of structural design, however, it is very frequent that a lack of information occurs about such randomness and this makes the fuzzy approach more meaningful for a consistent solution of the problem. Think for example to a beam imperfectly clamped at one end. This link is usually modeled through a rotational spring having uncertain stiffness. The translation of this problem in probabilistic terms is not simple, since no information are usually available about the random distribution of the stiffness value. Conversely, it appears more direct and reasonable to consider a band of situations between the hinged and the clamped ones, which defines a design domain large enough to include the actual one under investigation. Situations of weak structural coupling are very frequent in structural engineering, as for instance happens for structures built in subsequent phases, for large span cable supported bridges and for high rise buildings.

For these reasons, in the present study the uncertainties are modeled by using a fuzzy criterion in which the model is defined through bands of values, bounded between suitable minimum and maximum extremes. The reliability problem is formulated at the load level, with reference to several serviceability and ultimate limit states. For the critical interval associated to each limit state, the membership function of the safety factor is derived by solving a corresponding anti-optimization problem. The planning of this solution process is governed by a genetic algorithm, which generates the sampling values of the parameters involved by the material and geometrical non-linear structural analyses.

The effectiveness of the proposed approach and its capability to handle complex structural systems are shown by carrying out a reliability assessment of a prestressed concrete continuous beam and of a cable-stayed bridge.

2. Handling uncertainty in structural engineering

2.1. Randomness vs fuzziness

The uncertainties associated to a physical phenomena may derive from several and different sources. In the common language, something is uncertain when it assumes random meanings or behaviors (*randomness*), or when it is not clearly established or described (*vagueness*), or when it may have more than one possible meaning or status (*ambiguity*), or, finally, when it is described on the basis of too limited amount of information (*imprecision*). At a closer examination, *randomness*, *vagueness*, *ambiguity*, and *imprecision* denote uncertainties with different and specific characteristics: for *randomness* the source of uncertainty is due to intrinsic factors related to the physics of the phenomena, which determine the events under investigation; in the other cases the source of uncertainty arises from the limited capacity of our formal languages to describe the engineering problem to be solved (*ambiguity*), or from incorrect and/or ill-posed definitions of quantities which convey some informative content (*vagueness*), or from some lack of knowledge (*imprecision*).

The last three aspects have subjective nature and are usually included in the wider concept of *fuzziness*, which, in this sense, results in juxtaposition with the objective concept of *randomness*. Randomness and fuzziness have also complementary definitions. A given event is called *random* or *deterministic* if it is affected or not, respectively, by randomness. In an analogous way, the same event can be called *fuzzy* or *crisp* if it is affected or not,

respectively, by fuzziness. It is obvious that both types of uncertainty are always involved in real engineering problems, even if in different measure, depending on the circumstances [20]. Despite of this evidence, in civil engineering fuzziness tends to be fully neglected, or at most improperly treated like randomness in the context of the probability theory. Clearly, a more rational way to handle all kinds of uncertainty requires the formulation of specific methodologies and procedures also within the framework of the fuzzy theory [10,19]. The development of an effective fuzzy approach to structural reliability is then the first fundamental step towards a more meaningful mixed probabilistic–fuzzy measure of safety, where randomness and fuzziness are contemporarily accounted for in a proper way [15].

2.2. Membership functions and uncertainty levels

In set theory, based on classical logic, an element x of the universe of discourse X can belong or not to a given set $A \subseteq X$, in the sense that the membership conditions are mutually exclusive between them (Fig. 1a). A *crisp* set A can then be described by a membership function $\mu = \mu_A(x)$, which coincides with the set indicator function as defined in standard topology and which is stated as follows:

$$\mu_A(x) = \begin{cases} 1 & \text{if } x \in A, \\ 0 & \text{if } x \notin A, \end{cases} \quad \forall x \in X \tag{1}$$

However, in linguistic terms there are sets that cannot be considered as crisp. As an example, one can consider the sets of "tall" and "short" people: since the limits of such sets cannot be defined with precision, one person can be considered as belonging to both of them, at least in a *certain measure*. Fuzzy logic allows us to consider such aspects and to develop a wider and more general fuzzy sets theory which includes the classical theory as a limit situation [6,21]. In particular, the membership function $\mu = \mu_{\tilde{A}}(x)$ of a fuzzy set $\tilde{A} \subseteq X$ assigns to each element x a degree of membership varying in the closed interval $[0; 1]$ (Fig. 2b), or:

$$0 \leqslant \mu_{\tilde{A}}(x) \leqslant 1, \quad \forall x \in X \tag{2}$$

In other words, a fuzzy membership function is a *possibilistic* distribution suitable to describe uncertain information, when a probabilistic distribution is not directly available. Of course, the construction of this possibilistic function is based on subjective criteria, but it is not arbitrary, since it clearly depends on the specific context of the problem.

Analogously to the probabilistic case, in fuzzy structural analysis the membership functions of the input data must be processed in order to achieve the corresponding membership functions of the output parameters which define the structural response. To this aim, it is useful to discretize the continuous fuzzy variables by choosing some levels of membership $\alpha \in [0, 1]$, called α-levels, which represent different levels of uncertainty (Fig. 2). In this way, the relationships among fuzzy sets can be studied by using the usual

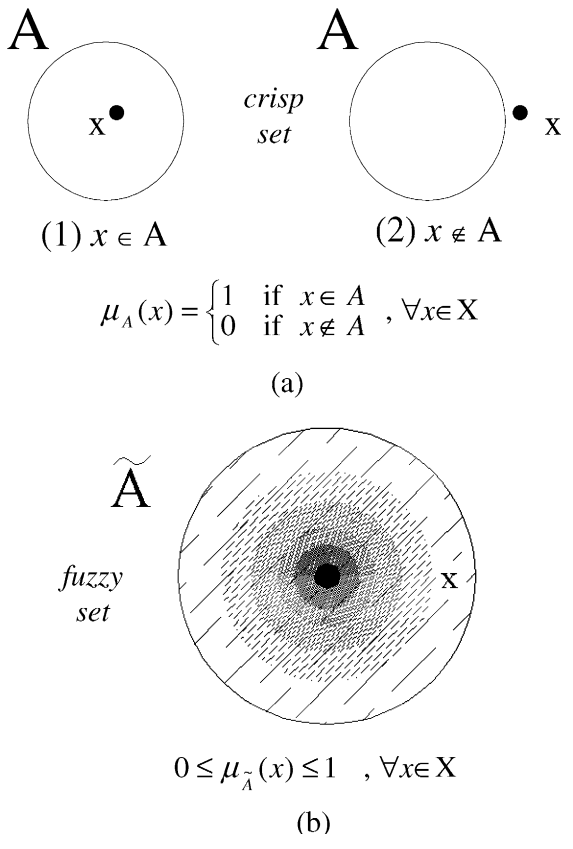

Fig. 1. Membership rules for (a) crisp and (b) fuzzy sets.

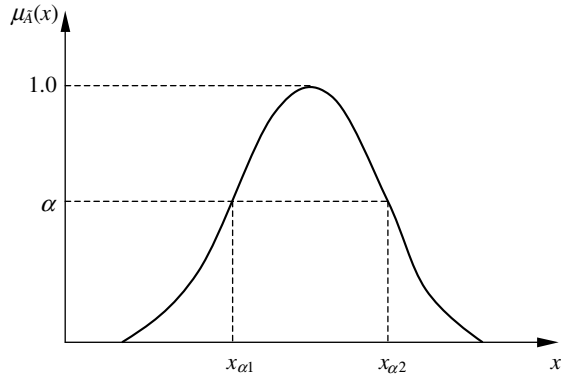

Fig. 2. Membership function and α-levels.

concepts of classical logic and the methodologies of the interval analysis, applied to each α-level.

2.3. Interval analysis and anti-optimization of the structural response

Let x be a parameter belonging to the set of quantities which define the structural problem and λ a load multiplier. It is clear that to each set of parameters corresponds a set of limit load multipliers λ_F, one of them for each assigned limit state.

For the sake of simplicity, we start our developments by considering the relationship between one single parameter x and one single limit state condition, defined by its corresponding limit load multiplier λ_F. It is worth noting that, in general, that relationship $\lambda_F = \lambda_F(x)$ is non-linear, even if the behavior of the system is linear. This is typical of design processes where the structural properties which correlate loads and displacements are considered as design variables. The implications of such a non-linearity can be outlined with reference to the schematic graph, shown in Fig. 3. In a deterministic analysis, to each singular value of the parameter x corresponds a singular value of the value of the multiplier λ_F (Fig. 3a). In fuzzy analysis we need to relate the interval of uncertainty on x, associated to a given α-level, to the corresponding response interval on λ_F. Such problem is not straightforward, since the response interval $[\lambda_{F\min}; \lambda_{F\max}]$ corresponding to $[x_{\min}; x_{\max}]$ cannot be simply obtained from $\lambda_F(x_{\min})$ and $\lambda_F(x_{\max})$, how Fig. 3b highlights [13]. Moreover, in real applications the number of uncertain parameters tends to be very high and the problem of finding the interval response may become extremely complex.

In this paper such a problem is properly formulated as an optimization problem by assuming the objective function $F(x)$ to be maximized as the size of the response interval itself, or $F(x) = [\lambda_{F\max}(x) - \lambda_{F\min}(x)]$ (see Fig. 3b). In particular, for the general case of n independent parameters x, collected in a vector $\mathbf{x} = [x_1 \;\; x_2 \;\; \ldots \;\; x_n]^{\mathrm{T}}$, and m assigned limit states, the following objective function is introduced:

$$F(\mathbf{x}) = \sum_{i=1}^{m} [\lambda^i_{F\max}(\mathbf{x}) - \lambda^i_{F\min}(\mathbf{x})] \tag{3}$$

As an alternative, since from the structural safety point of view the lower bounds $\lambda_{F\min}$ of the response intervals only are often of interest, the following form of the objective function can be also assumed:

$$F(\mathbf{x}) = \sum_{i=1}^{m} [\lambda^i_0 - \lambda^i_{F\min}(\mathbf{x})] \tag{4}$$

where λ_0 is a constant value properly chosen, for example in such a way that $F(\mathbf{x}) \geqslant 0$. Since the worst structural configurations are looked for, the previous formulation leads to a so-called anti-optimization problem.

The solution $\mathbf{x}$ of the anti-optimization problem which takes the side constraints $\mathbf{x}_{\min} \leqslant \mathbf{x} \leqslant \mathbf{x}_{\max}$ into account, is developed by genetic algorithms. Genetic algorithms are heuristic search techniques which belong to the class of stochastic algorithms, since they combine elements of deterministic and probabilistic search. More

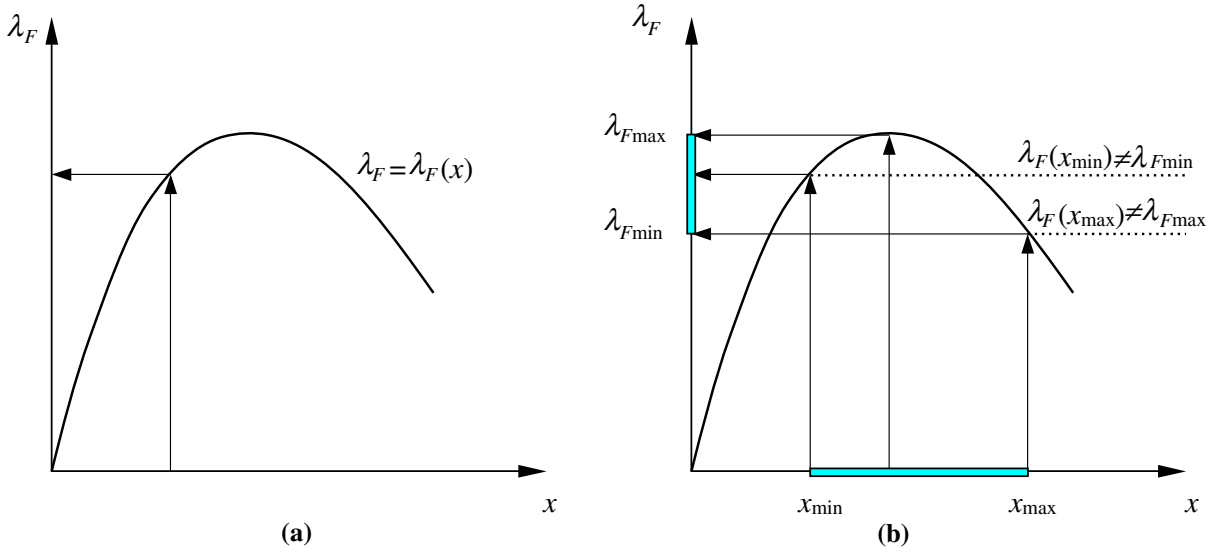

Fig. 3. (a) Non-linear relationship between a structural parameter x and the limit load multiplier λ_F associated to the violation of a given limit state. (b) Mapping between the interval of uncertainty on x and the corresponding response interval on λ_F.

properly, the search strategy works on a *population* of *individuals* subjected to an evolutionary process, where individuals compete between them to survive in proportion to their *fitness* with the *environment*. In this process, the population undergoes continuous reproduction by means of some *genetic operators* which, because of competition, tend to preserve the best individuals. From this evolutionary mechanism, two conflicting trends appear: the exploitation of the best individuals and the exploration of the environment. Thus, the effectiveness of the genetic search depends on a balance between them, or between two principal properties of the system, *population diversity* and *selective pressure*. These aspects are in fact strongly related, since an increase in the selective pressure decreases the diversity of the population, and vice versa [18].

With reference to the optimization problem previously formulated, a population of m individuals belonging to the environment $E = \{\mathbf{x}|\mathbf{x}^- \leqslant \mathbf{x} \leqslant \mathbf{x}^+\}$ represents a collection $X = \{\mathbf{x}_1 \quad \mathbf{x}_2 \quad \dots \quad \mathbf{x}_m\}$ of m possible solutions $\mathbf{x}_k^{\mathrm{T}} = [x_1^k \quad x_2^k \quad \dots \quad x_n^k] \in E$, each defined by a set of n design variables x_i^k $(k = 1, \dots, m)$. To assure an appropriate hierarchical arrangement of the individuals, their fitness $F(\mathbf{x}) \geqslant 0$, which increases with the adaptability of $\mathbf{x}$ to its environment E, should be properly scaled. More details about the adopted scaling rules, internal coded representation of the population, genetic operators and termination criteria, can be found in a previous paper [1].

3. Non-linear analysis of reinforced and prestressed concrete framed structures

The standard design of reinforced and prestressed concrete frames is usually based on a linear elastic analysis under several load combinations and on a subsequent set of non-linear cross-sectional verifications. This kind of approach is simple, but contains some intrinsic inconsistencies in particular with respect to the use of global safety factors which affect not only the safety measurements, but also the results of the analyses in terms of both displacements and internal stresses [14].

When realistic results are needed, material and geometrical non-linearity must be taken into account directly, in a full non-linear analysis, and the structural safety must be directly evaluated at the load level. Many reports and codes of practice recognize these aspects and highlight how the non-linear analysis can give more meaningful results than usual linear analysis (see for example [12]).

Without any loss of generality, this study focuses on concrete framed structures for which shear and connection failures are assumed to be avoided by a proper capacity design. In such a context, the structural modeling is based on a two-dimensional reinforced/prestressed concrete finite beam element whose formulation deals with both the mechanical non-linearity, associated to the constitutive laws of the materials (concrete, ordinary and prestressing steels), and the geometrical non-linearity, due to second order effects induced by the change of configuration of the beam [7,8,17]. The two-dimensional formulation presented in this paper is thought for monotonic static loading. A three-dimensional formulation of such an element for cyclic dynamic loading can be found in [2].

3.1. Formulation of the reinforced concrete finite beam element

We refer to technical beam theory applied to the beam finite element shown in Fig. 4. The strain field over the cross-sections is derived on the basis of the Bernoulli–Navier hypothesis which assumes a linear distribution of normal strains. The only active strain and stress components are the longitudinal elongation ε_x and the corresponding stress σ_x. No shear strain and stress are considered. Based on such hypotheses, the vector of the displacements (axial u and transversal v):

$$\mathbf{u} = [\,u(x) \quad v(x)\,]^{\mathrm{T}} \tag{5}$$

and the vector of the generalized strains (axial strain ε_0 and curvature χ):

$$\boldsymbol{\varepsilon} = [\,\varepsilon_0(x) \quad \chi(x)\,]^{\mathrm{T}}, \quad \varepsilon_0 = \frac{\partial u}{\partial x}, \quad \chi = \frac{\partial^2 v}{\partial x^2} \tag{6}$$

depend on the vector of the nodal displacements:

$$\mathbf{q} = [\,u_i \quad u_j \;\vdots\; v_i \quad \varphi_i \quad v_j \quad \varphi_j\,]^{\mathrm{T}} \tag{7}$$

as follows:

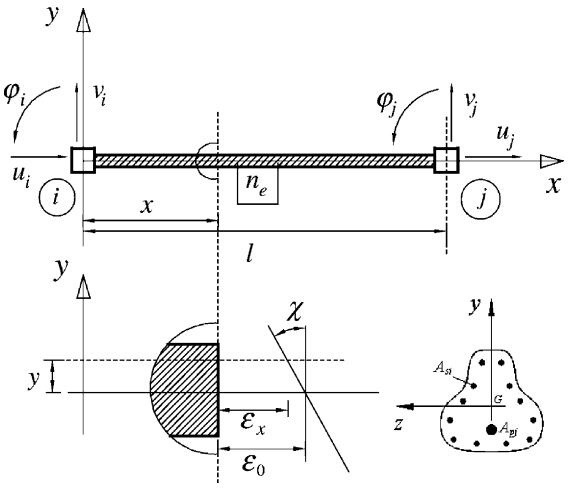

Fig. 4. Reinforced/prestressed finite beam element.

$$\mathbf{u} = \mathbf{N}\mathbf{q} \tag{8}$$

$$\mathbf{N} = \left[\begin{array}{c|c} \mathbf{N}_a & \mathbf{0} \\ \hline \mathbf{0} & \mathbf{N}_b \end{array}\right] = \left[\begin{array}{cc|cccc} N_1(x) & N_2(x) & 0 & 0 & 0 & 0 \\ \hline 0 & 0 & N_3(x) & N_4(x) & N_5(x) & N_6(x) \end{array}\right] \tag{9}$$

$$\boldsymbol{\varepsilon} = \mathbf{B}\mathbf{q} \tag{10}$$

$$\mathbf{B} = \left[\begin{array}{c|c} \mathbf{B}_a & \mathbf{0} \\ \hline \mathbf{0} & \mathbf{B}_b \end{array}\right] = \left[\begin{array}{c|c} \partial\mathbf{N}_a/\partial x & \mathbf{0} \\ \hline \mathbf{0} & \partial^2\mathbf{N}_b/\partial x^2 \end{array}\right] \tag{11}$$

where $N_k(x)$, with $k = 1, \ldots, 6$, are the axial $\mathbf{N}_a$ and bending $\mathbf{N}_b$ displacement functions of a linear elastic beam element having uniform cross-sectional stiffness and loaded only at its ends ($\xi = x/l$):

$$N_1(\xi) = 1 - \xi, \quad N_2(\xi) = \xi \tag{12a}$$

$$N_3(\xi) = 1 - 3\xi^2 + 2\xi^3, \quad N_4(\xi) = (\xi - 2\xi^2 + \xi^3)l \tag{12b}$$

$$N_5(\xi) = 3\xi^2 - 2\xi^3, \quad N_6(\xi) = (-\xi^2 + \xi^3)l \tag{12c}$$

Moreover, calling $\mathbf{L} = [\,1 \quad -y\,]$, the normal strain $\varepsilon_x = \varepsilon_x(x, y)$ of the fiber at the distance y from the beam axis can be expressed as:

$$\varepsilon_x = \mathbf{L}\boldsymbol{\varepsilon} = \mathbf{L}\mathbf{B}\mathbf{q} \tag{13}$$

We consider the structure in equilibrium under the external applied forces and the corresponding internal stress field. For any variation of the actual displacement field, which comply with both the internal and external compatibility, the Principle of Virtual Displacements states that the internal work δL_i equals the external one δL_e due to (a) the nodal loads $\mathbf{F}_0 = [\,\mathbf{F}_{0a} \quad \mathbf{F}_{0b}\,]^\mathrm{T} = [\,F_{xi} \quad F_{xj} \,|\, F_{yi} \quad M_i \quad F_{yj} \quad M_j\,]^\mathrm{T}$, (b) the loads $\mathbf{f} = [\,f_x(x) \quad f_y(x)\,]^\mathrm{T}$ distributed along the beam, and (c) the nodal forces $\mathbf{Q} = [\,\mathbf{Q}_a \quad \mathbf{Q}_b\,]^\mathrm{T} = [\,Q_1 \quad Q_2 \,|\, Q_3 \quad Q_4 \quad Q_5 \quad Q_6\,]^\mathrm{T}$ through which the beam interacts with the structure:

$$\delta L_\mathrm{e} = \delta W_F + \delta W_f + \delta W_Q \tag{14a}$$

$$\delta W_F = \delta\mathbf{q}^\mathrm{T}\mathbf{F}_0 \tag{14b}$$

$$\delta W_f = \int_0^l \delta\mathbf{u}^\mathrm{T}\mathbf{f}\,\mathrm{d}x = \delta\mathbf{q}^\mathrm{T}\int_0^l \mathbf{N}^\mathrm{T}\mathbf{f}\,\mathrm{d}x = \delta\mathbf{q}^\mathrm{T}\mathbf{F}_1 \tag{14c}$$

$$\delta W_Q = \delta\mathbf{q}^\mathrm{T}\mathbf{Q} \tag{14d}$$

The internal work is written in secant form. With reference to a generic non-linear elastic material, the uniaxial stress–strain constitutive law is expressed as follows:

$$\sigma_x = \sigma_x(\varepsilon_x) = \overline{E}\varepsilon_x \tag{15}$$

where $\overline{E} = \overline{E}(\varepsilon_x)$ is the secant modulus of the material. The corresponding internal work results:

$$\begin{aligned}\delta L_\mathrm{i} &= \int_V \delta\varepsilon_x\sigma_x\,\mathrm{d}V = \int_V \delta\varepsilon_x\overline{E}\varepsilon_x\,\mathrm{d}V \\ &= \int_V \delta\mathbf{q}^\mathrm{T}\mathbf{B}^\mathrm{T}\mathbf{L}^\mathrm{T}\overline{E}\mathbf{L}\mathbf{B}\mathbf{q}\,\mathrm{d}V \\ &= \delta\mathbf{q}^\mathrm{T}\left\{\int_0^l \mathbf{B}^\mathrm{T}\left(\int_A \overline{E}\mathbf{h}\,\mathrm{d}A\right)\mathbf{B}\,\mathrm{d}x\right\}\mathbf{q} \\ &= \delta\mathbf{q}^\mathrm{T}\left\{\int_0^l \mathbf{B}^\mathrm{T}\overline{\mathbf{H}}\mathbf{B}\,\mathrm{d}x\right\}\mathbf{q} = \delta\mathbf{q}^\mathrm{T}\overline{\mathbf{K}}_\mathrm{M}\mathbf{q}\end{aligned} \tag{16}$$

where $\mathbf{h} = \mathbf{h}(y) = \mathbf{L}(y)^\mathrm{T}\mathbf{L}(y)$ and $\overline{\mathbf{K}}_\mathrm{M}$ is the corresponding secant stiffness matrix due to materials. In particular, by denoting respectively with:

$$\overline{E}_\mathrm{c} = \overline{E}_\mathrm{c}(\varepsilon_\mathrm{c}) = \frac{\sigma_\mathrm{c}(\varepsilon_\mathrm{c})}{\varepsilon_\mathrm{c}} \tag{17a}$$

$$\overline{E}_{si} = \overline{E}_{si}(\varepsilon_{si}) = \frac{\sigma_{si}(\varepsilon_{si})}{\varepsilon_{si}} \tag{17b}$$

the secant moduli of the concrete fiber at the depth y and of the the ith steel bar placed at the depth y_i, with $i = 1, \ldots, n_\mathrm{b}$, and calling A_c and A_{si} the corresponding areas of the concrete matrix and of the ith steel bar, the secant stiffness matrix $\overline{\mathbf{H}} = \overline{\mathbf{H}}(x, \mathbf{q})$ of the composite cross-section can be expressed as:

$$\begin{aligned}\overline{\mathbf{H}} &= \int_A \overline{E}\mathbf{h}\,\mathrm{d}A = \int_{A_\mathrm{c}} \overline{E}_\mathrm{c}\mathbf{h}_\mathrm{c}\,\mathrm{d}A \\ &\quad + \sum_{i=1}^{n_\mathrm{b}} \overline{E}_{si}\mathbf{h}_{si}A_{si} = \overline{\mathbf{H}}_\mathrm{c} + \overline{\mathbf{H}}_\mathrm{s}\end{aligned} \tag{18}$$

where $\mathbf{h}_\mathrm{c} = \mathbf{h}(y)$ and $\mathbf{h}_{si} = \mathbf{h}(y_i)$.

Finally, the equilibrium condition of the beam element can be derived from the virtual displacement equation $\delta L_\mathrm{i} = \delta L_\mathrm{e}$:

$$\overline{\mathbf{K}}_\mathrm{M}\mathbf{q} = \mathbf{F}_0 + \mathbf{F}_1 + \mathbf{Q} \tag{19}$$

with $\overline{\mathbf{K}}_\mathrm{M} = \overline{\mathbf{K}}_\mathrm{M}(\mathbf{q})$. In this way, the material non-linearities associated to both concrete matrix and reinforcing steel bars are introduced. It is worth noting that such kind of non-linearities leads to a coupling between axial and bending behavior.

3.2. Geometrical stiffness

Let P be an axial force applied to the ends of the beam element, and let Δ be the corresponding displacement (Fig. 5). This displacement is congruent with

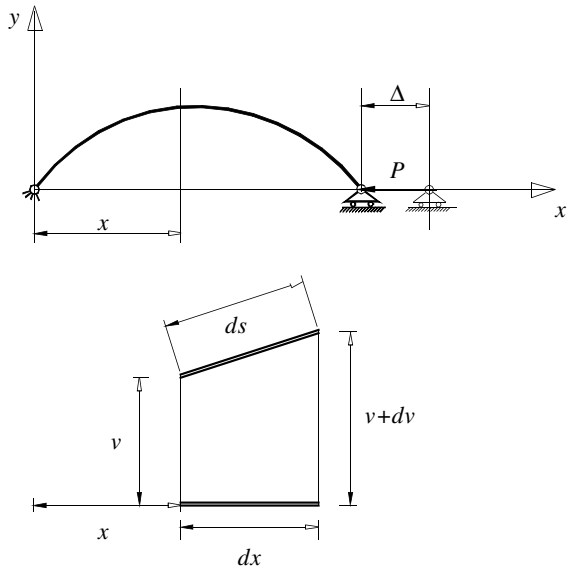

Fig. 5. Second order geometrical non-linearity.

the deformed shape and equals the difference between the length of the bent beam, assumed as axially rigid, and the length of the cord of its deformed axis:

$$\mathrm{d}s = \sqrt{\mathrm{d}x^2 + \mathrm{d}v^2} = \left[1 + \frac{1}{2}\left(\frac{\mathrm{d}v}{\mathrm{d}x}\right)^2 - \frac{1}{4}\left(\frac{\mathrm{d}v}{\mathrm{d}x}\right)^4 + \cdots\right]\mathrm{d}x \tag{20a}$$

$$\mathrm{d}s - \mathrm{d}x = \frac{1}{2}\left(\frac{\mathrm{d}v}{\mathrm{d}x}\right)^2 \mathrm{d}x + \mathrm{O}\left[\left(\frac{\mathrm{d}v}{\mathrm{d}x}\right)^4\right] \tag{20b}$$

Neglecting the higher order terms and adopting the beam's displacement functions in the following form:

$$\frac{\mathrm{d}v}{\mathrm{d}x} = \left[\mathbf{0} \;\vdots\; \frac{\partial \mathbf{N}_b}{\partial x}\right]\mathbf{q} = \mathbf{G}\mathbf{q} \tag{21}$$

we obtain:

$$\Delta = \int_0^l (\mathrm{d}s - \mathrm{d}x) = \frac{1}{2}\int_0^l \left(\frac{\mathrm{d}v}{\mathrm{d}x}\right)^2 \mathrm{d}x = \frac{1}{2}\mathbf{q}^{\mathrm{T}} \int_0^l \mathbf{G}^{\mathrm{T}}\mathbf{G}\,\mathrm{d}x\,\mathbf{q} \tag{22}$$

or:

$$\delta\Delta = \delta\mathbf{q}^{\mathrm{T}} \int_0^l \mathbf{G}^{\mathrm{T}}\mathbf{G}\,\mathrm{d}x\,\mathbf{q} \tag{23}$$

From the corresponding virtual work:

$$\delta W = -P\delta\Delta = -\delta\mathbf{q}^{\mathrm{T}} P \int_0^l \mathbf{G}^{\mathrm{T}}\mathbf{G}\,\mathrm{d}x\,\mathbf{q} = -\delta\mathbf{q}^{\mathrm{T}}\mathbf{K}_{\mathrm{G}}\mathbf{q} \tag{24}$$

the well known geometric stiffness matrix $\mathbf{K}_{\mathrm{G}} = \mathbf{K}_{\mathrm{G}}(\mathbf{q})$ is then derived:

$$\mathbf{K}_G = -P\int_0^l \mathbf{G}^T\mathbf{G}\,\mathrm{d}x = \frac{-P}{30l}\left[\begin{array}{cc:cccc} 0 & 0 & 0 & 0 & 0 & 0 \\ 0 & 0 & 0 & 0 & 0 & 0 \\ \hdashline 0 & 0 & 36 & 3l & -36 & 3l \\ 0 & 0 & 3l & 4l^2 & -3l & -l^2 \\ 0 & 0 & -36 & -3l & 36 & -3l \\ 0 & 0 & 3l & -l^2 & -3l & 4l^2 \end{array}\right] \tag{25}$$

The equilibrium condition of the beam element can be rewritten by taking the geometrical non-linearity into account as well:

$$(\overline{\mathbf{K}}_{\mathrm{M}} + \mathbf{K}_{\mathrm{G}})\mathbf{q} = \mathbf{F}_0 + \mathbf{F}_1 + \mathbf{Q} \tag{26}$$

3.3. Prestressing

The total strain of a cable is given by two contributions: the assigned initial prestressing strain and the strain compatible with the deformation of the concrete matrix. In the following, it will be shown that the strain due to compatibility leads to a modification of the stiffness matrix, as for the reinforcing steel, while the initial prestressing strain leads to a vector of nodal forces equivalent to the prestressing action.

The beam element is assumed to be prestressed by $i = 1, \ldots, n_{\mathrm{c}}$ cables having the eccentricity $e_i = e_i(\xi)$ with respect to the beam axis. Let ε_i be the strain at the depth of the ith cable:

$$\varepsilon_i = \varepsilon(e_i) = \mathbf{L}_{\mathrm{P}i}\boldsymbol{\varepsilon} = \mathbf{L}_{\mathrm{P}i}\mathbf{B}\mathbf{q} \tag{27}$$

where $\mathbf{L}_{\mathrm{P}i} = \mathbf{L}(e_i)$. At first, we assume that the cables are adherent to the concrete matrix, as usual for pre-tensioned elements. In such hypothesis, by denoting with $\varepsilon_{\mathrm{P}0i}$ the contribution to the strain of the ith cable due only to the prestressing, after both the instantaneous and time-dependent losses are discounted, the total strain of the cable is:

$$\varepsilon_{\mathrm{P}i} = \varepsilon_{\mathrm{P}0i} + \varepsilon_i \tag{28}$$

In this way, by denoting:

$$\overline{E}_{\mathrm{P}i} = \overline{E}_{\mathrm{P}i}(\varepsilon_{\mathrm{P}i}) = \frac{\sigma_{\mathrm{P}i}(\varepsilon_{\mathrm{P}i})}{\varepsilon_{\mathrm{P}i}} \tag{29}$$

the secant modulus of the prestressing steel, the corresponding stress in the cable $\sigma_{\mathrm{P}i}$ can be written as follows:

$$\sigma_{\mathrm{P}i} = \frac{\sigma_{\mathrm{P}i}}{\varepsilon_{\mathrm{P}i}} \cdot \varepsilon_{\mathrm{P}i} = \overline{E}_{\mathrm{P}i}(\varepsilon_{\mathrm{P}0i} + \varepsilon_i) \tag{30}$$

With reference to a field of virtual displacements $\delta\mathbf{q}$, the internal work associated to the prestressing can be thus evaluated:

$$\begin{aligned}\delta L_{\mathrm{i}} &= \int_V \delta\varepsilon\sigma_{\mathrm{P}}\,\mathrm{d}V = \int_0^l \sum_{i=1}^{n_{\mathrm{c}}} \delta\varepsilon_i\sigma_{\mathrm{P}i}A_{\mathrm{P}i}\,\mathrm{d}x \\ &= \int_0^l \sum_{i=1}^{n_{\mathrm{c}}} \delta\varepsilon_i\overline{E}_{\mathrm{P}i}(\varepsilon_{\mathrm{P}0i}+\varepsilon_i)A_{\mathrm{P}i}\,\mathrm{d}x \\ &= \delta\mathbf{q}^{\mathrm{T}}\left\{\int_0^l \mathbf{B}^{\mathrm{T}}\sum_{i=1}^{n_{\mathrm{c}}}\mathbf{L}_{\mathrm{P}i}^{\mathrm{T}}\overline{E}_{\mathrm{P}i}\varepsilon_{\mathrm{P}0i}A_{\mathrm{P}i}\,\mathrm{d}x\right\} \\ &\quad + \delta\mathbf{q}^{\mathrm{T}}\left\{\int_0^l \mathbf{B}^{\mathrm{T}}\sum_{i=1}^{n_{\mathrm{c}}}\overline{E}_{\mathrm{P}i}A_{\mathrm{P}i}\mathbf{h}_{\mathrm{P}i}\mathbf{B}\,\mathrm{d}x\right\}\mathbf{q} \\ &= -\delta\mathbf{q}^{\mathrm{T}}\mathbf{F}_{\mathrm{P}} + \delta\mathbf{q}^{\mathrm{T}}\left\{\int_0^l \mathbf{B}^{\mathrm{T}}\overline{\mathbf{H}}_{\mathrm{P}}\mathbf{B}\,\mathrm{d}x\right\}\mathbf{q} \\ &= \delta\mathbf{q}^{\mathrm{T}}(-\mathbf{F}_{\mathrm{P}} + \overline{\mathbf{K}}_{\mathrm{P}}\mathbf{q})\end{aligned} \tag{31}$$

with $\mathbf{h}_{\mathrm{P}i} = \mathbf{h}(e_i)$ and where the matrices $\overline{\mathbf{H}}_{\mathrm{P}} = \overline{\mathbf{H}}_{\mathrm{P}}(x,\mathbf{q})$ and $\overline{\mathbf{K}}_{\mathrm{P}} = \overline{\mathbf{K}}_{\mathrm{P}}(\mathbf{q})$ are the contributions of the cables to the secant stiffness matrix of the cross-section x and of the beam respectively, while $\mathbf{F}_{\mathrm{P}} = \mathbf{F}_{\mathrm{P}}(\mathbf{q})$ is the vector of the nodal forces equivalent to the prestressing. Therefore, the equilibrium equations can be rewritten in the following form:

$$(\overline{\mathbf{K}}_{\mathrm{M}} + \mathbf{K}_{\mathrm{G}} + \overline{\mathbf{K}}_{\mathrm{P}})\mathbf{q} = \mathbf{F}_0 + \mathbf{F}_1 + \mathbf{F}_{\mathrm{P}} + \mathbf{Q} \tag{32}$$

The previous developments directly apply to pre-tensioned elements, in which the cables are always adherent to the concrete matrix. Additional considerations are due for post-tensioned elements, where the cables are unbounded either during the first stage of prestressing, or even for the whole service life of the structure. In fact, when the cables are unbounded the prestressing induces only a system of forces $\mathbf{F}_{\mathrm{P}}$. The cables and the beam are compatible only at the ends and the prestressing does not interfere with the cross-sectional stiffness ($\mathbf{K}_{\mathrm{P}} = \mathbf{0}$). Subsequently, if the ducts are filled, the grouting enforces the compatibility along the cable as well and induces a change in the stiffness properties of the beam element ($\mathbf{K}_{\mathrm{P}} \neq \mathbf{0}$). Starting from this new initial state, the structural analysis proceeds as previously described for the pre-tensioned elements.

3.4. Constitutive laws

According to the assumed hypotheses, we refer to suitable uniaxial stress–strain relationships [9]. The stress–strain diagram of the concrete is shown in Fig. 6a. The branch in compression is described by Saenz as follows:

$$\sigma_{\mathrm{c}} = \frac{k\eta - \eta^2}{1 + (k-2)\eta}, \quad \varepsilon_{\mathrm{cu}} \leqslant \varepsilon_{\mathrm{c}} \leqslant 0 \tag{33}$$

where $k = E_{\mathrm{c0}}\varepsilon_{\mathrm{c1}}/f_{\mathrm{c}}$, and $\eta = \varepsilon_{\mathrm{c}}/\varepsilon_{\mathrm{c1}}$. The branch in tension is defined by an elastic–perfectly plastic model. The stress–strain diagram of reinforcing steel is assumed elastic perfectly-plastic in both tension and in compression (Fig. 6b), while for prestressing steel the plastic branch is assumed as non-linear and is described by the following fifth order degree polynomial function (Fig. 6c):

$$\varepsilon_{\mathrm{p}} = \frac{\sigma_{\mathrm{p}}}{E_{\mathrm{p}}} + 0.823\frac{|\varepsilon_{\mathrm{p}}|}{\varepsilon_{\mathrm{p}}}\left(\frac{|\sigma_{\mathrm{p}}|}{f_{\mathrm{py}}} - 0.7\right)^5, \quad \varepsilon_{\mathrm{py}} \leqslant |\varepsilon_{\mathrm{p}}| \leqslant \varepsilon_{\mathrm{pu}} \tag{34}$$

3.5. Numerical integration

The characteristics of the reinforced/prestressed concrete beam finite element must be obtained from the numerical computation of the integrals previously introduced. With this regard, it is worth noting that the finite element presented in the present paper is different from the so-called fiber elements [11], since the numerical integration is performed by higher order rules. In

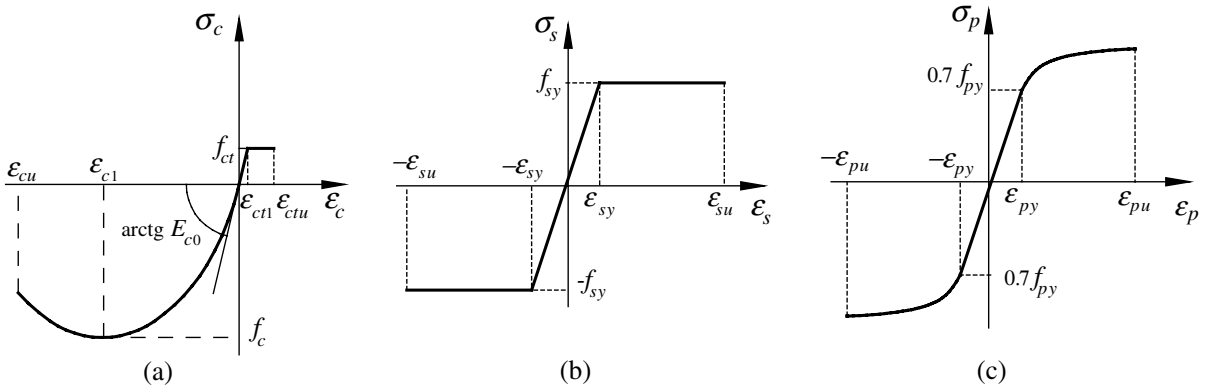

Fig. 6. Constitutive laws of the materials: (a) concrete, (b) reinforcing and (c) prestressing steel.

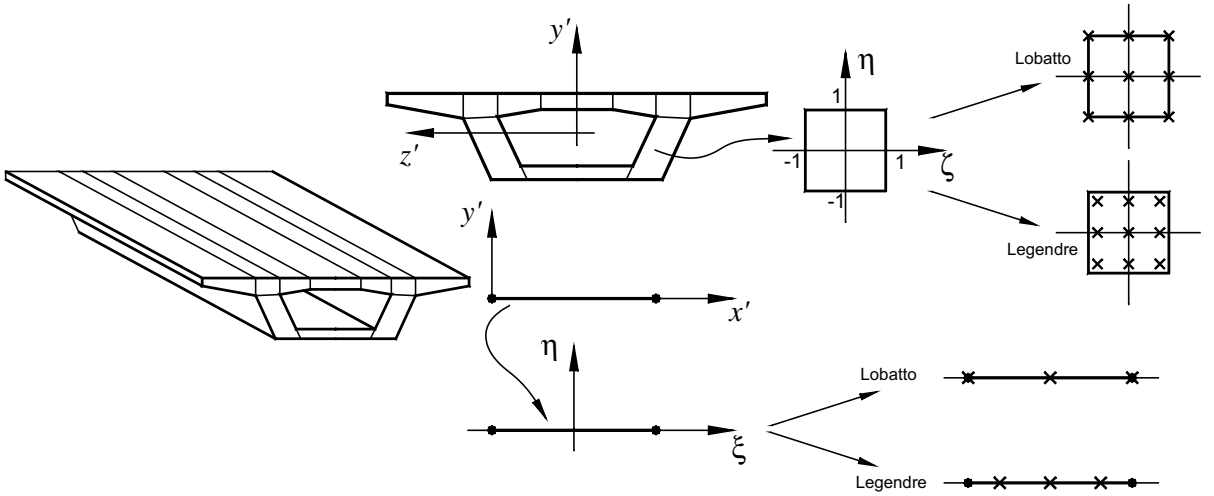

Fig. 7. Subdivision of the finite element volume in isoparametric subdomains and locations of the Gauss integration points according to both the Legendre and Lobatto rules.

particular, the area of the beam cross-section is firstly subdivided in four-nodes isoparametric subdomains, and a Gauss–Legendre and/or a Gauss–Lobatto numerical integration is performed over each subdomain and then along the whole element (Fig. 7).

3.6. Overall equilibrium

Finally, both the secant stiffness matrix $\overline{\mathbf{K}} = \overline{\mathbf{K}}_{\mathrm{M}} + \mathbf{K}_{\mathrm{G}} + \overline{\mathbf{K}}_{\mathrm{P}}$ and the vector of the total nodal forces $\mathbf{F} = \mathbf{F}_0 + \mathbf{F}_1 + \mathbf{F}_{\mathrm{P}}$ of each element must be assembled over the whole structure with reference to a global coordinate system. Since the overall contribution of the vectors $\mathbf{Q}$ vanishes, the equilibrium equations of the whole structure can be formally expressed again as follows:

$$\mathbf{R} = \overline{\mathbf{K}}\mathbf{q} = \mathbf{F} \tag{35}$$

For monotonic loads, the previous equations can be effectively solved numerically through the secant iterative technique shown in Fig. 8a, where both the restoring forces $\mathbf{R} = \mathbf{R}(\mathbf{q})$ and the applied loads $\mathbf{F} = \mathbf{F}(\mathbf{q})$ are depending on the unknown displacements $\mathbf{q}$.

4. Measure of the structural performance

4.1. Basic limit states of failure

Based on the general concepts of reinforced and prestressed concrete design, structural performances should generally be described with reference to a specified set of limit states, with regards to both serviceability and ultimate conditions [9]: such limits separate desired states of the structure from undesired ones.

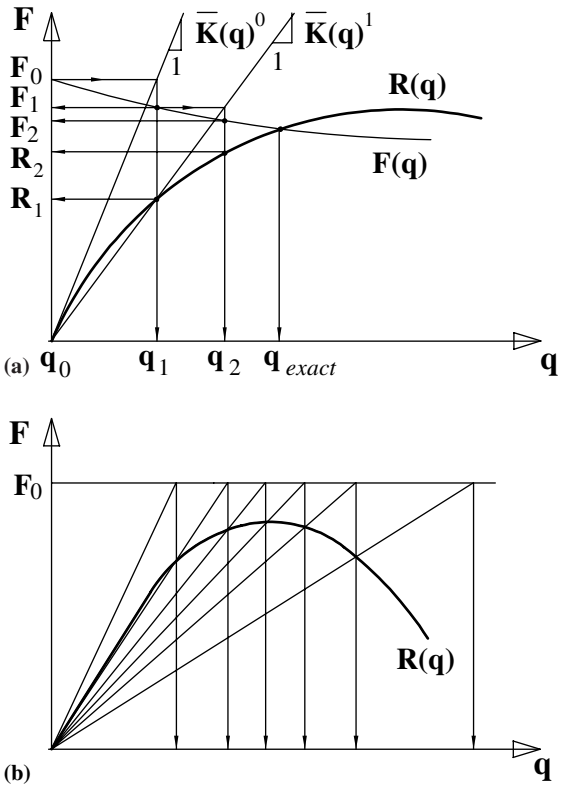

Fig. 8. Secant iterative technique for the solution of non-linear analysis problems. (a) Convergence in the general case $\mathbf{R}(\mathbf{q}) = \mathbf{F}(\mathbf{q})$, and (b) divergence for $\mathbf{R}(\mathbf{q}) = \mathbf{F}_0$.

Splitting cracks and considerable creep effects may occur if the compression stresses σ_c in concrete are too high. Besides, excessive stresses either in reinforcing steel σ_s or in prestressing steel σ_p can lead to unacceptable crack patterns. Excessive displacements $\mathbf{q}$ may also involve loss of serviceability and thus have to be limited within assigned bounds $\mathbf{q}^-$ and $\mathbf{q}^+$. Based on these considerations, the following limitations account for adequate durability at the serviceability stage (*Serviceability Limit States*):

$$\text{S1}: \quad -\sigma_c \leqslant -\alpha_c f_c \tag{36a}$$

$$\text{S2}: \quad |\sigma_s| \leqslant \alpha_s f_{sy} \tag{36b}$$

$$\text{S3}: \quad |\sigma_p| \leqslant \alpha_p f_{py} \tag{36c}$$

$$\text{S4}: \quad \mathbf{q}^- \leqslant \mathbf{q} \leqslant \mathbf{q}^+ \tag{36d}$$

where α_c, α_s and α_p are suitable reduction factors of the material strengths f_c, f_{sy} and f_{py}.

When the strain in concrete ε_c, or in the reinforcing steel ε_s, or in the prestressing steel ε_p reaches a limit value ε_{cu}, ε_{su} or ε_{pu}, respectively, the collapse of the corresponding cross-section occurs. However, the collapse of a single cross-section does not necessarily lead to the collapse of the whole structure, since the latter is caused by the loss of equilibrium arising when the reactions $\mathbf{R}$ requested for the loads $\mathbf{F}$ can no longer be developed (see Fig. 8b). Thus, the following basic ultimate conditions have to be verified (*Ultimate Limit States*):

$$\text{U1}: \quad -\varepsilon_c \leqslant -\varepsilon_{cu} \tag{37a}$$

$$\text{U2}: \quad |\varepsilon_s| \leqslant \varepsilon_{su} \tag{37b}$$

$$\text{U3}: \quad |\varepsilon_p| \leqslant \varepsilon_{pu} \tag{37c}$$

$$\text{U4}: \quad \mathbf{F} \leqslant \mathbf{R} \tag{37d}$$

Additional limit states of failure may also be introduced, depending on the nature of the specific structural problem under investigation.

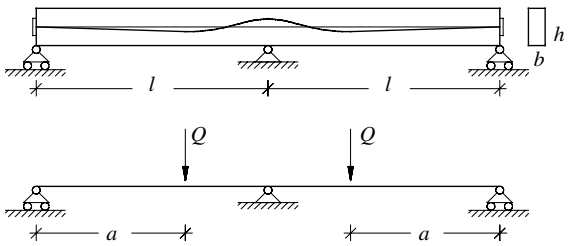

Fig. 9. Prestressed two-span continuous beam [16]. Cable profile and load condition.

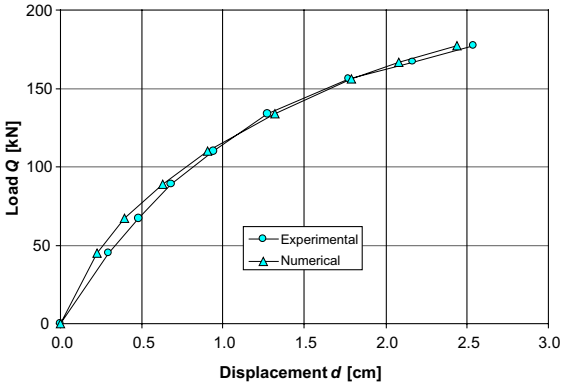

Fig. 10. Diagrams of the live load Q vs the corresponding displacement d at the middle span: comparison between numerical and experimental results.

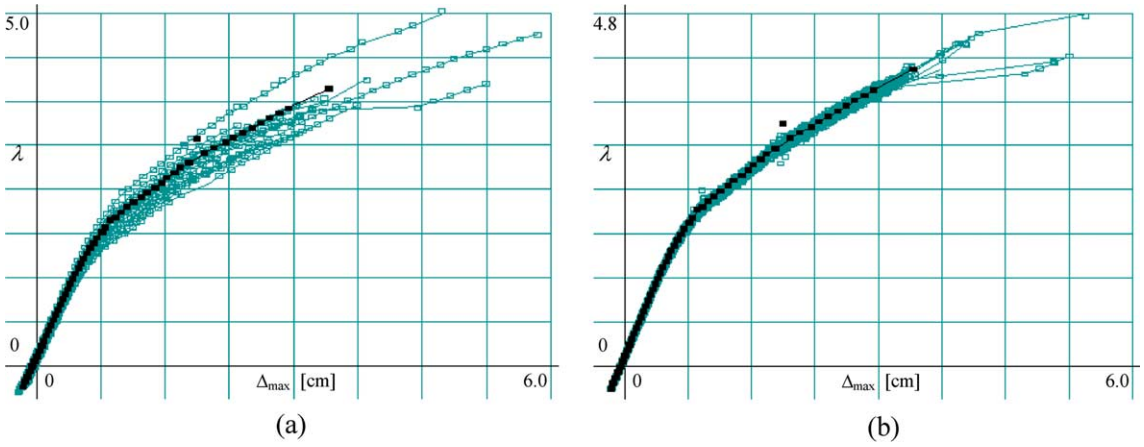

Fig. 11. Diagrams of the load multiplier λ vs the maximum displacement Δ_{max} for the nominal structure (black—■) and for some fuzzy simulations (gray—□) associated to the α-levels (a) [0.70–1.30], and (b) [0.95–1.05].

4.2. Load multiplier and safety factor

The limit state functions $h(\mathbf{y}) \leqslant 0$ previously introduced refer to internal quantities of the system $\mathbf{y}$. Since the relationship $\mathbf{y} = \mathbf{y}(\mathbf{x})$ between such quantities and the fuzzy variables $\mathbf{x}$ is generally available only in an implicit form, a check of the structural performance needs to be carried out at the load level. To this aim, it is

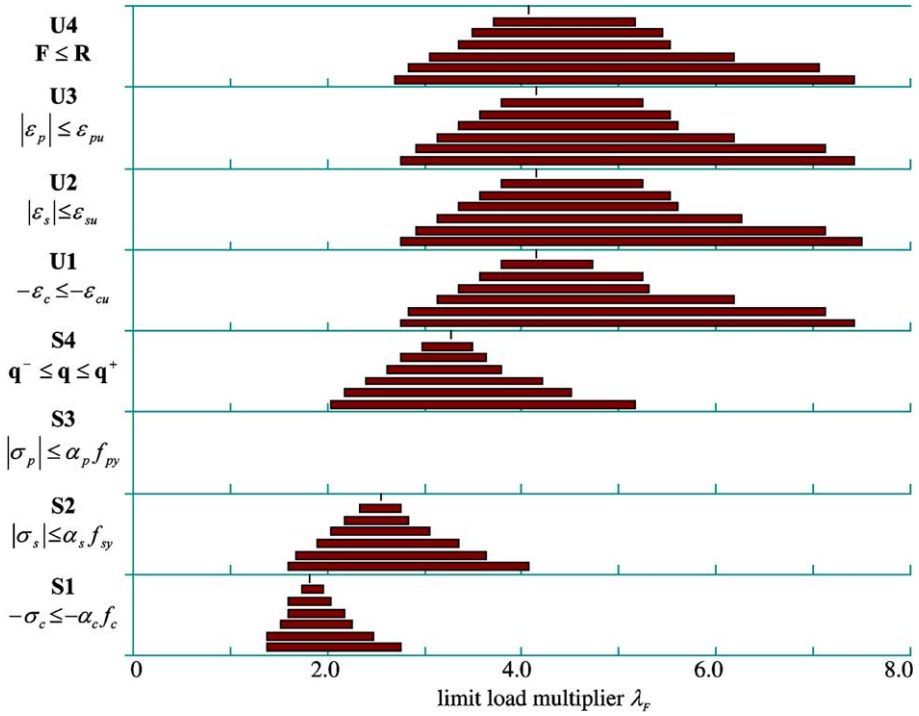

Fig. 12. Membership functions of the limit load multiplier at failure for each limit state. The response interval for each α-level has been obtained from a genetically driven anti-optimization process.

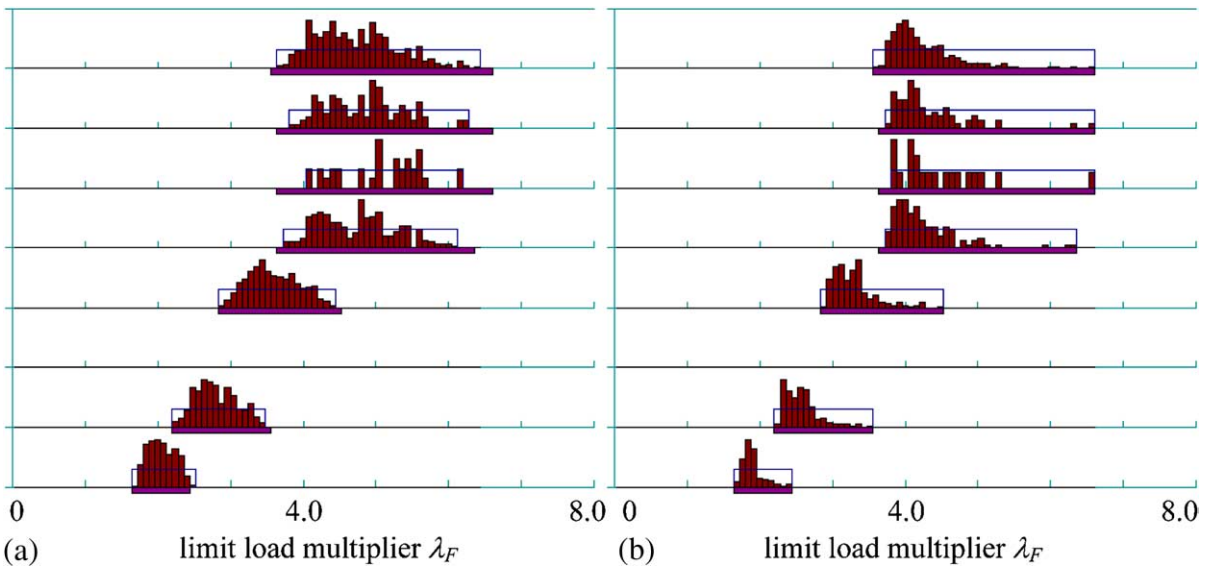

Fig. 13. Histograms of the limit load multiplier λ_F after about 400 simulations. (a) Random choice of data. (b) Genetically driven simulation.

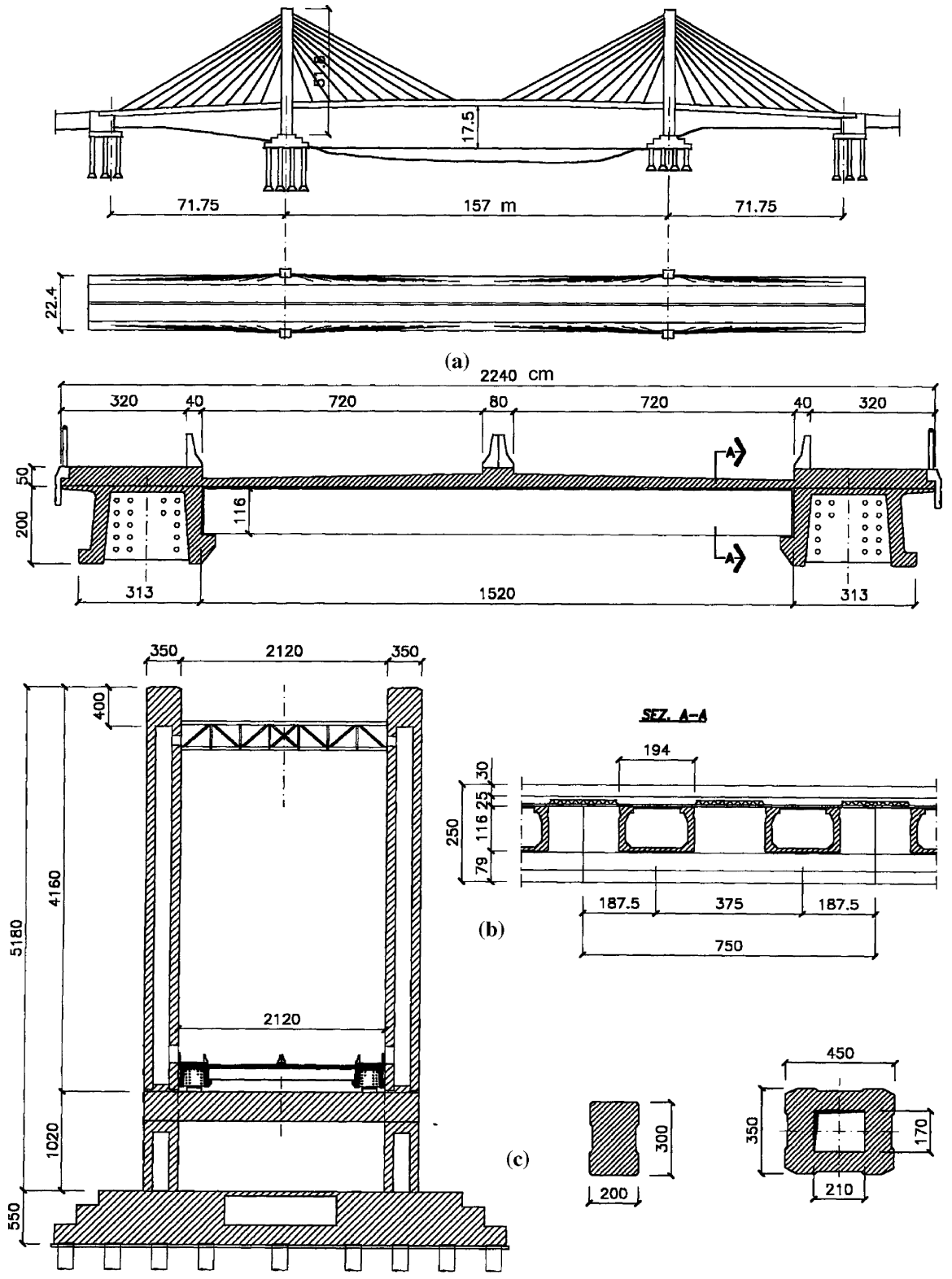

Fig. 14. Cable-stayed bridge over Cujaba River in Brazil. (a) Longitudinal view and main geometrical dimensions of the bridge. Sectional views of (b) the deck and (c) the pylons.

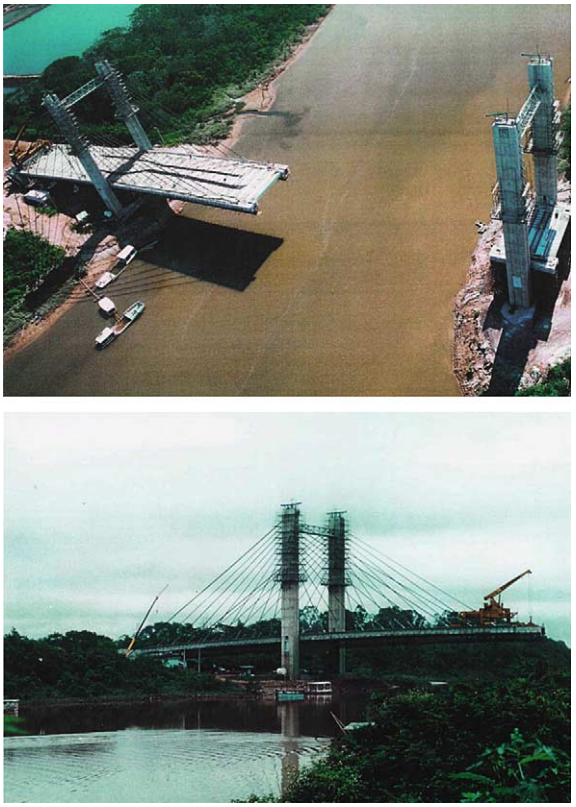

Fig. 15. Cable-stayed bridge over Cujaba River in Brazil. Two photographic views of the bridge during construction.

useful to assume $\mathbf{F} = \mathbf{G} + \lambda\mathbf{Q}$, where $\mathbf{G}$ is a vector of dead and prestressing loads and $\mathbf{Q}$ a vector of live loads whose intensity varies proportionally to a unique scalar multiplier $\lambda \geqslant 0$. In this context, the limit load multiplier $\lambda = \lambda_F$ associated to the violation of a limit state of failure, assumes the role of safety factor and the reliability of the structure against the nominal value of the loads has to be verified directly by checking the following limit state condition:

$$\lambda_F \geqslant \lambda_{\max} \tag{38}$$

where $\lambda_{\max}$ is a limit threshold of the load multiplier associated to each given limit state.

5. Applications

In the following, the fuzzy reliability analysis is used to model the structural behavior a prestressed concrete continuous beam and to support the design decisions regarding a segmentally erected cable-stayed bridge.

The first application regards a test beam, experimented by Lin [16], and intends to show, for a relatively simple structure, the level of detail allowed by non-linear analysis, the good accordance between experimental and numerical results and the effects due to the fuzziness of input data on the structural response.

The second application intends to show how such analyses can be performed also on relatively complex structures and how they allow us to support the design decision through a whole estimation of the structural behavior in presence of many and critical sources of fuzziness.

5.1. Prestressed concrete continuous beam

The two-span post-tensioned concrete continuous beam shown in Fig. 9 is considered [16]. The span length is $l = 7500$ mm, and the dimensions of the rectangular cross-section are $b = 203.2$ mm and $h = 406.4$ mm. The beam is reinforced with 2 bars $\varnothing 14$ mm ($A_{s1} = 153.9$ mm^2) placed at both the top and bottom edge with a cover $c = 32.4$ mm. The prestressing steel cable consists of 32 wires $\varnothing 5$ mm ($A_{p1} = 19.6$ mm^2) adherent to the concrete, having a straight profile from the ends of the beam ($e_1 = 0$) to the middle of its spans ($e_2 = -50$ mm), and a parabolic profile from these points to the middle support ($e_3 = 88$ mm). After the time-dependent losses, the nominal prestressing force at the beam ends is $P_{\text{nom}} = 527.5$ kN. This force decreases along the beam because of the losses due to friction. A curvature friction coefficient $\mu = 0.3$ and a wobble friction coefficient $K = 0.0016$ rad/m have been assumed. The nominal values material properties are:

$$f_{\text{c,nom}} = -41.3 \text{ MPa}, \quad \varepsilon_{\text{c1}} = -2‰, \quad \varepsilon_{\text{cu}} = -3.4‰, \quad \varepsilon_{\text{ctu}} = 2\varepsilon_{\text{ct1}} \tag{39a}$$

$$f_{\text{sy,nom}} = 314 \text{ MPa}, \quad E_{\text{s}} = 196 \text{ GPa}, \quad \varepsilon_{\text{su}} = 16\% \tag{39b}$$

$$f_{\text{py,nom}} = 1480 \text{ MPa}, \quad E_{\text{p}} = 200 \text{ GPa}, \quad \varepsilon_{\text{pu}} = 1\% \tag{39c}$$

Table 1
Design values of the material properties and levels of prestressing

Concrete peak strength (deck)	f_{c}	−22.6 MPa
Concrete peak strength (pylons)	f_{c}	−19.8 MPa
Concrete peak strain	ε_{c1}	−0.002
Concrete ultimate strain	ε_{cu}	−0.0035
Reinforcing steel strength	f_{sy}	383 MPa
Reinforcing steel Young modulus	E_{s}	205 GPa
Reinforcing steel ultimate strain	ε_{su}	0.01
Prestressing steel strength	f_{py}	1617 MPa
Prestressing steel Young modulus	E_{p}	195 GPa
Prestressing steel ultimate strain	ε_{pu}	0.015
Prestressing stress (deck)	σ_{po}	1000 MPa
Prestressing stress (stays)	σ_{po}	500 MPa

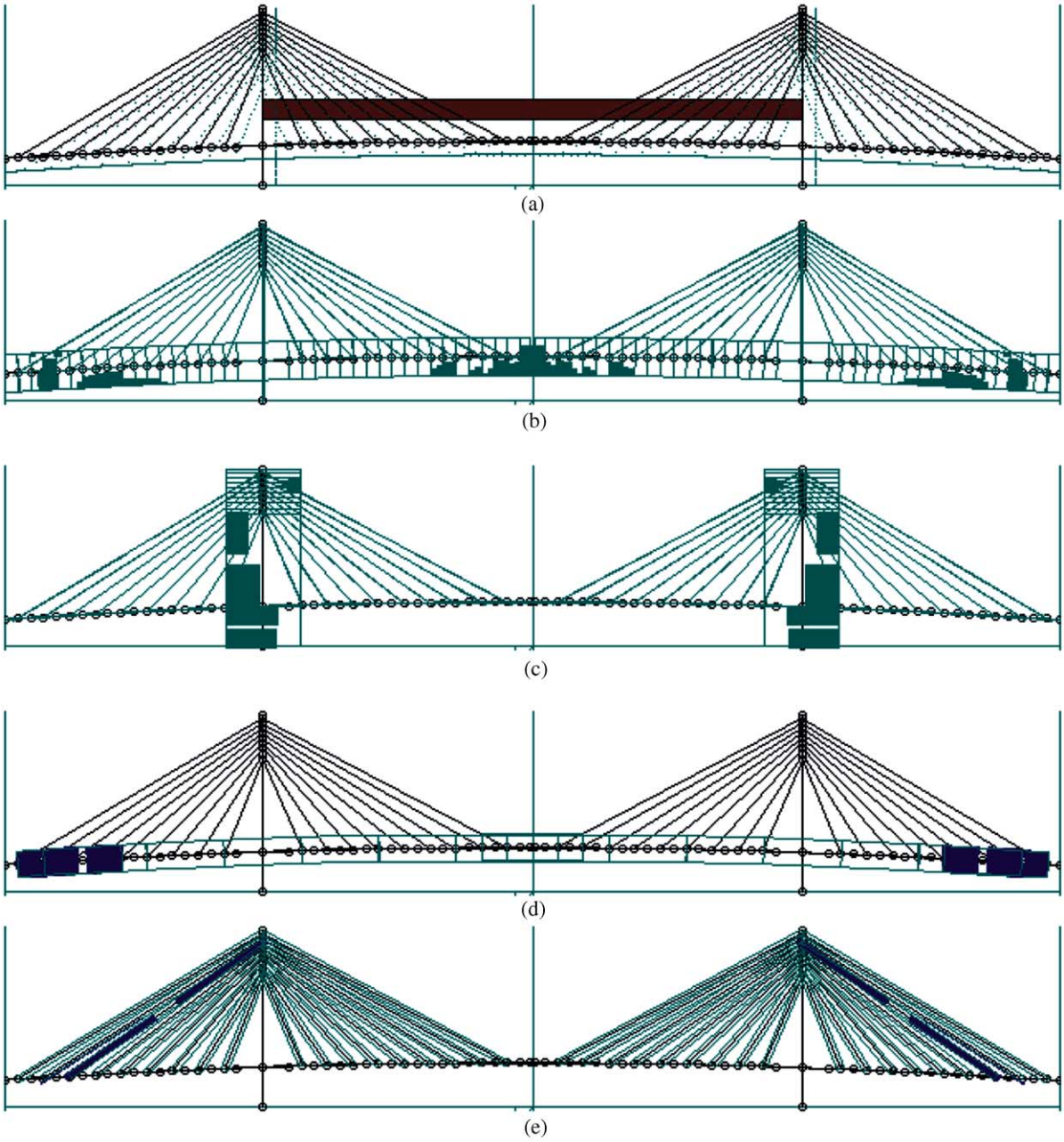

Fig. 16. Step-by-step non-linear analysis of the cable-stayed bridge (nominal structure) under the dead loads and a live load uniformly distributed over the whole central span. (a) Two-dimensional model of the bridge. Distributed of cracking (shaded area) at collapse in both (b) the deck and (c) the pylons. Slackness in both (d) the segment of the deck and (e) the stays.

with a weight density of the composite material $\gamma = 25$ kN/m^3. Besides the self-weight, the beam is loaded with two concentrated loads having nominal value $Q_{\text{nom}} = 50$ kN and placed at the distance $a = 4880$ mm from each end, as shown in Fig. 9. For this load condition, the serviceability limit states are detected assuming $\alpha_c = 0.45$, $\alpha_s = 0.80$, $\alpha_p = 0.75$, $q^+ = -q^- = l/400$.

The reliability analysis is carried out assuming the following quantities as uncertain:

- the strengths of concrete and of both reinforcing and prestressing steel for each of the 10 finite elements that compose the beam (30 variables);

- the prestressing force of the strands (1 variable);
- the value of the live loads (1 variable).

These 32 fuzzy variables $\mathbf{x} = [x_1 \quad x_2 \quad \dots \quad x_{32}]^T$ are assumed to have a triangular membership function with unit height for the nominal value x_{nom} and interval base $[0.70–1.30]x_{nom}$. Seven α-levels of membership are considered, corresponding to the followings dimensionless intervals of uncertainty:

$[0.70–1.30] = \pm 30$
$[0.75–1.25] = \pm 25\%$
$[0.80–1.20] = \pm 20\%$
$[0.85–1.15] = \pm 15\%$
$[0.90–1.10] = \pm 10\%$
$[0.95–1.05] = \pm 5\%$
$[1.00–1.00] = \pm 0\%$

Fig. 10 allows us to appreciate the good accordance of the non-linear analysis of the nominal structure with the experimental results. The diagrams in Fig. 11 show the interval response obtained from some simulations associated to the α-levels [0.70–1.30] and [0.95–1.05], respectively. The membership functions of the limit load multipliers λ_F associated to the basic limit states previously defined are finally presented in Fig. 12, where the response interval for each α-level has been obtained from a genetically driven anti-optimization process. Assuming a limit threshold $\lambda_{max} = 1$ the limit states are not violated and the structure is safe. For increasing values of the limit threshold λ_{max} the violation of the third serviceability limit state S3 (concerning the stress in the reinforcing bars) never appears, while for the other limit states the spread of the uncertainty can be appreciated, especially for the larger α-levels. With this regard, it is worth noting that uncertainties larger than 15% seems to appear critical, in particular for the ultimate limit states. Finally, the effectiveness of the genetic algorithm in driving the simulation process should be highlighted. Fig. 13 shows the histograms of the limit

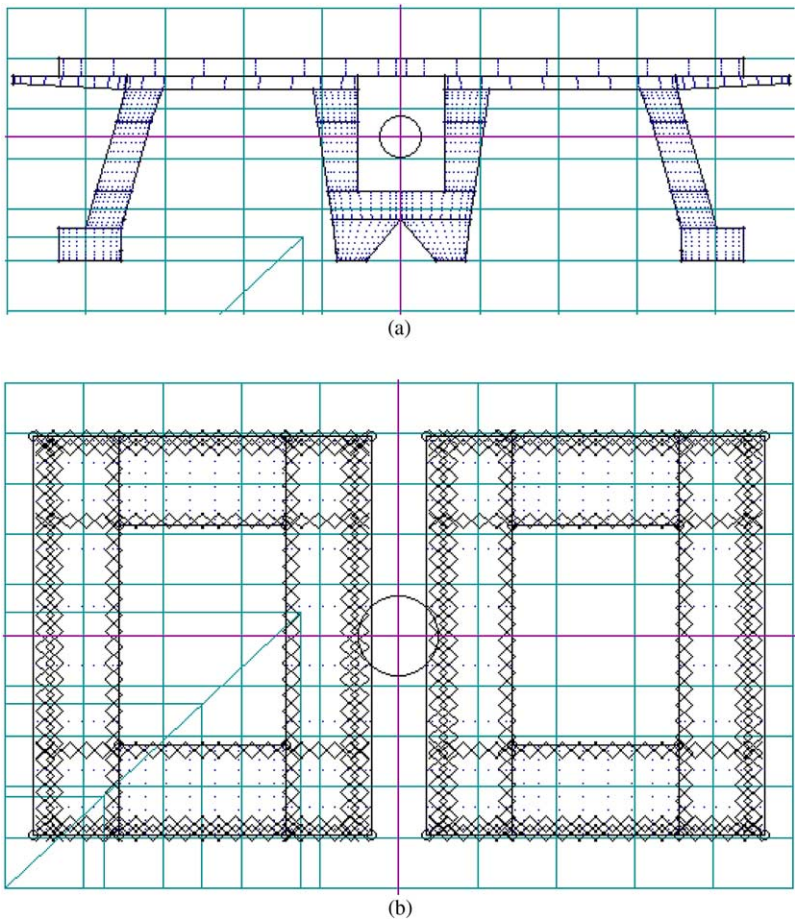

Fig. 17. Model of the typical cross-section of both (a) the deck and (b) the pylons. Subdivision of the concrete area and distribution of both the reinforcement bars and the prestressing cables.

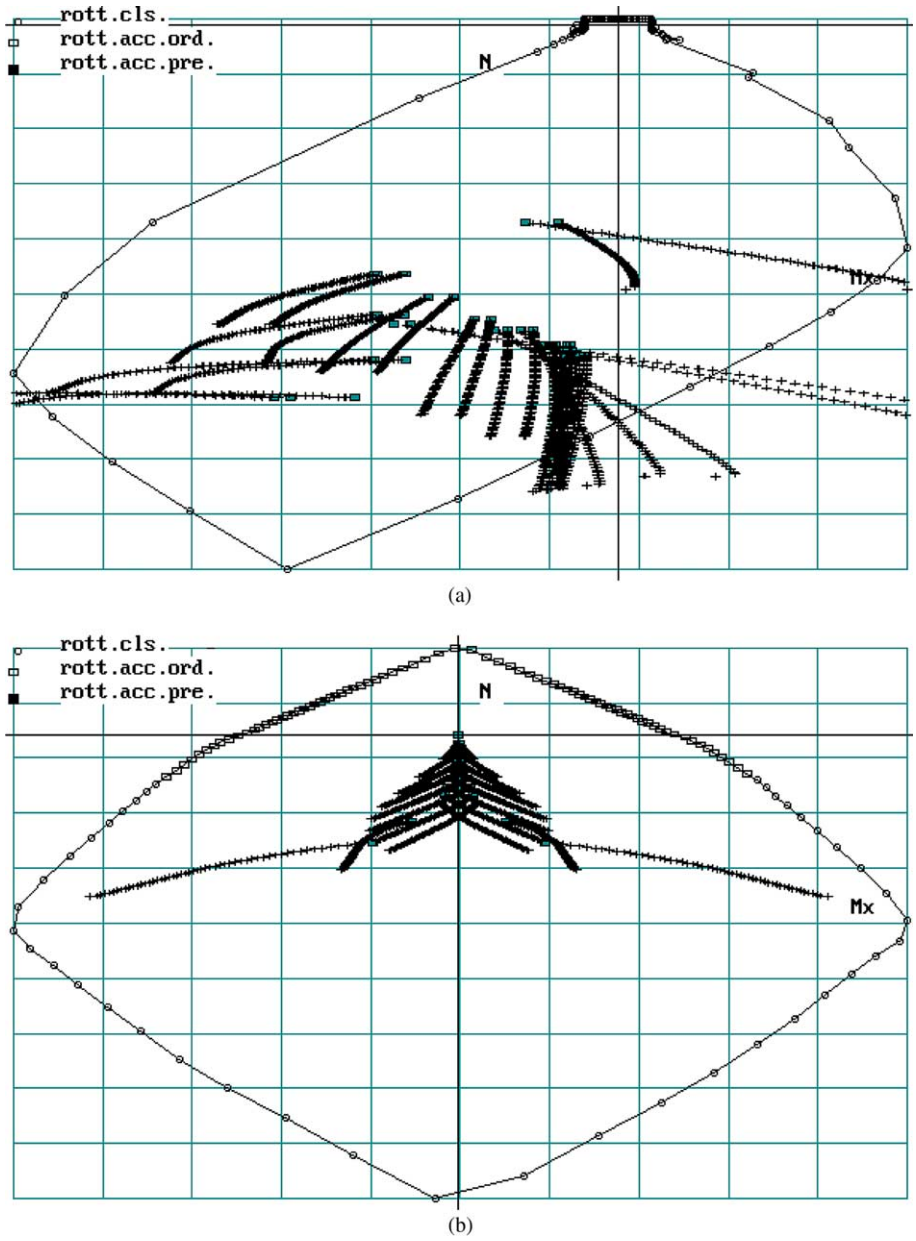

Fig. 18. Bending moment (horizontal axis)–axial force (vertical axis) limit state curves for both (a) the deck and (b) the pylons. In the diagrams are also plotted the load points corresponding to the evolution of the stress in the Gauss section of the structure for the loading case of Fig. 15.

load multiplier λ_F resulting from a sample of about 400 simulations, performed for a given α-level and by assuming alternatively: (a) a purely random choice of data, and (b) a genetically driven simulation. A comparison of the results leads us to the appreciation of the higher capability of the genetic search in exploring the regions of the response interval where the limit state violations tends to occur with higher frequency.

5.2. Cable-stayed bridge

The second application concerns the sensitivity analyses carried out to support the design decisions regarding a cable-stayed bridge designed by the late Francesco Martinez y Cabrera and recently built over Cujaba River in Brazil (Figs. 14 and 15). The pylons of the bridge are cast-in-place, while the deck is completely

precast and subdivided in 80 segments which are connected between themselves only by the shear friction assured by the prestressing forces. The design values of the material properties and of the initial prestressing in both the deck and the pylons are listed in Table 1. Besides the dead load g due to the self-weight of the structural and non-structural members, a live load $q = 100$ kN/m applied along the bridge deck is considered.

To the aim of the reliability analysis, the following quantities are considered to be uncertain (see Table 1 for the nominal values):

- the strength of the concrete in each segment of the deck (80 variables) and in each pylon (2 variables);
- the prestressing force in each cable (32 variables);
- the prestressing force in each stay (78 variables);
- the live load acting on each segment of the deck (80 variables).

Such 272 variables $\mathbf{x} = [x_1 \quad x_2 \quad \dots \quad x_{272}]^{\mathrm{T}}$ are modeled using a fuzzy criterion. The 190 variables which describe the concrete strengths and the prestressing forces are continuous with a triangular membership function having unit height for the nominal value x_{nom} and interval base $[0.80\text{–}1.20]x_{\mathrm{nom}}$. The 80 variables associated to the live load are instead defined over the discrete set $[0; x_{\mathrm{nom}}]$ with the same degree of membership for both the values, which means that the nominal load may be present or not on each segment of the deck with the same level of uncertainty.

The reliability of the bridge with respect to the ultimate limit states only is investigated. Besides the basic failure criteria previously introduced, additional limit states are considered in order to account for the specific nature of the structural system. In particular, since the effectiveness of the connections between the segments which form the deck is depending on their level of compression, a limit state of decompression is assumed to be violated when the strain in concrete ε_{c} reaches a conventional strain limit in tension $\varepsilon_{\mathrm{d}} = 0.0002$. A higher degree of failure of the connection is also considered to occur when the amount of cracked area A_{cr} over a section reaches 1/3 of its total area A_{c}. Based on the same concept, also the slackness of the stays denote a failure condition which occurs when the strain in the steel ε_{p} is no longer positive. Based on the previous considerations, the following three additional ultimate limit states have to be verified:

$$\mathrm{U5}: \quad \varepsilon_{\mathrm{c}} \leqslant \varepsilon_{\mathrm{d}} \text{ (in the deck only)} \tag{40a}$$

$$\mathrm{U6}: \quad 3A_{\mathrm{cr}} \leqslant A_{\mathrm{c}} \text{ (in the deck only)} \tag{40b}$$

$$\mathrm{U7}: \quad -\varepsilon_{\mathrm{p}} \leqslant 0 \text{ (in the stays only)} \tag{40c}$$

For the non-linear analysis of the structure, the deck and the pylons are modeled by using the reinforced/prestressed finite beam element previously presented. The stays are instead modeled using a truss element having axial stiffness only if its total strain is non-negative. Besides the already mentioned mechanical and geometrical non-linearity, the formulation of such element takes also into account the characteristic tension-hardening behavior due to the change in sag of the stays. The contributes to the truss element stiffness matrix and to its nodal force vector are then derived in an analogous way like for the beam.

The two-dimensional model of the cable-stayed bridge is shown in Fig. 16, together with some of the results obtained by a step-by-step non-linear analysis based on the nominal value of the variables which define the structural system and assuming the live load as uniformly distributed over the whole central span. Fig. 17 shows a typical subdivision adopted for the cross-section of both the deck and the pylons, as well as the corresponding distribution of both the reinforcing bars and the prestressing cables. Moreover, Fig. 18 shows the bending moment–axial force interaction curves of both the deck and the pylons associated to the limit state of sectional failure (limit states U1, U2 and U3). In the same diagrams the point

Table 2
Limit values of the live load multiplier for different load conditions (nominal structure)

Limit state	1 λ_F	2 λ_F	3 λ_F	4 λ_F	$\lambda_{F\,\min}$
U1	10	5.5	5.7	–	5.5
U2	–	–	–	–	–
U3	–	5.5	–	–	5.5
U4	10	5.5	5.7	6.0	5.5
U5	4.1	1.6	1.7	1.9	1.6
U6	5.4	3.8	2.6	2.3	2.3
U7	–	5.5	5.7	5.9	5.5

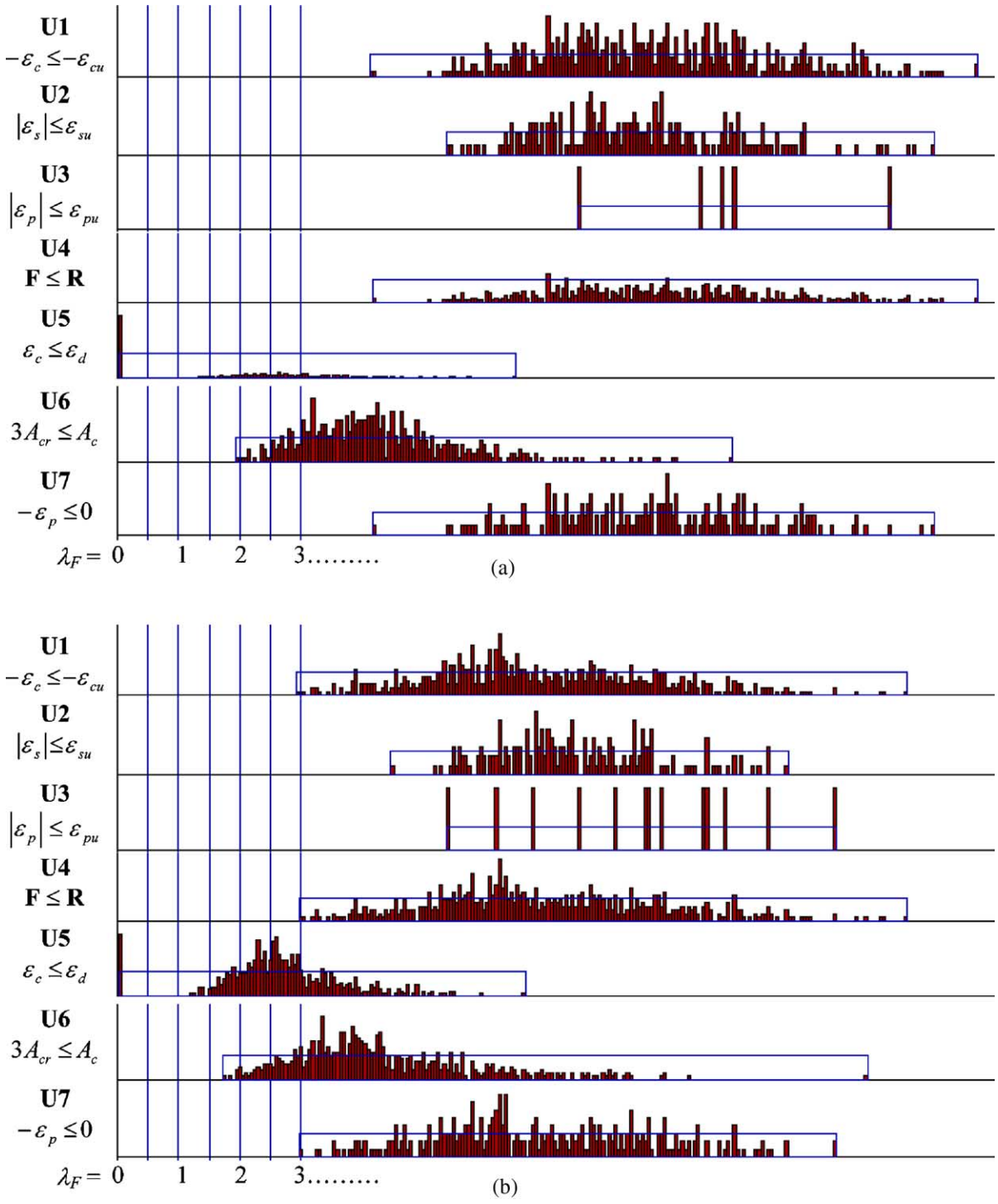

Fig. 19. Membership function of the load multiplier at failure for the α-level equal 0.5 derived by (a) a random sampling method, and (b) a genetically driven anti-optimization process (data samples of about 5000 simulations in both cases).

loads corresponding to the evolution of the stress state in the Gauss section of the structure are also plotted for the loading case shown in Fig. 16. The limit values of the live load multiplier associated to

several loading conditions are finally resumed in Table 2.

Based on the previously introduced models, a genetic anti-optimization problem has been solved for several α-levels. Fig. 19 shows the histograms of the limit load multiplier λ_F obtained for the α-level equal to 0.5, or by assuming the continuous fuzzy variables as varying in the interval $[0.90–1.10]x_{\text{nom}}$. For such level, the convergence of the search process has been achieved after a total of about 5000 simulations. First of all, Fig. 19 highlights the higher capability of the genetic search in exploring the regions of the failure domain associated to the lowest values of the minimum limit load multipliers. In fact, with respect to the histograms shown in Fig. 19a, deduced from a purely random search on a sample having the same size (about 5000 simulations), the histograms obtained by solving the anti-optimization problem and shown in Fig. 19b are translated on the left along the horizontal axis, or towards more critical configurations for the structure. Finally, the histograms of Fig. 19b show that, for the nominal value of the live load ($\lambda_{\max} = 1$), the monitored limit states seems to be fully verified with the exception of the case U5. With this regard, since the prestressing action tends to balance the dead loads, it is worth noting that some minor localized violations of the decompression condition of the deck for $\lambda = 0$ were expected and verified as not critical for the global reliability of the structure. Based on such considerations, the cable-stayed bridge appears to be safe with respect to the considered α-level. Analogous considerations can be made for other levels of uncertainty.

6. Conclusions

In this paper, a general methodology for the fuzzy reliability analysis of structural systems has been presented and specialized to the case of reinforced and prestressed concrete structures. The reliability problem is formulated at the load level and the membership function of the safety factor over the failure interval is derived for several limit states by solving the corresponding anti-optimization problems. Particular attention is paid to both the solution of the optimization process, based on a genetic algorithm, and the structural analysis techniques, which exploit the potentiality of a reinforced/prestressed beam finite element able to take both material and geometrical non-linearity into account. The results of two applications, one on a prestressed concrete continuous beam and the other on a cable-stayed bridge, show that the proposed procedure is effective both in easily handling implicit formulation of the performance relationships, as well as in performing system-level evaluations even for large structures.

As a concluding remark, it is worth noting that the proposed fuzzy approach should not be considered as alternative to a purely probabilistic formulation, given that the two methods account for different aspects of the same problem. In fact, as known, the fuzzy theory allows a treatment of uncertainty due to lacks of information, while the probability theory is based on a perfect knowledge about the stochastic variability resulting from the random nature of the same quantities. However, it also have to be noted that an autonomous approach to the reliability structural assessment, like the probabilistic formulation proposed by the codes, should find a higher rationality in a fuzzy approach which, due either to the real nature of the involved uncertainties, or to a higher simplicity of the mathematical formulation, seems to be more suitable for design purposes.

Acknowledgements

This paper is dedicated to the memory of Francesco Martinez y Cabrera, formerly professor of "Theory and Design of Bridge Structures" at the Technical University of Milan, who started us to a comprehensive vision of structures and life.

References

[1] Biondini F. Optimal limit state design of concrete structures using genetic algorithms. Studies and researches, vol. 20. School for Concrete Structures "Fratelli Pesenti", Politecnico di Milano, 1999. p. 1–30.
[2] Biondini F. Bridges structures under seismic actions. Modeling and optimization. PhD thesis, Politecnico di Milano, 2000 (in Italian).
[3] Biondini F, Bontempi F, Malerba PG. Fuzzy theory and genetically-driven simulation in the reliability assessment of concrete structures. In: Proceedings of 8th ASCE Joint Specialty Conference on Probabilistic Mechanics and Structural Reliability, University of Notre Dame (IN), July 24–26, 2000.
[4] Biondini F, Bontempi F, Malerba PG, Martinez y Cabrera F. Reliability assessment of cable-stayed bridges. In: Proceedings of IABSE Conference on Cable-Supported Bridges Seoul, Korea, June 12–14, 2001.
[5] Blockley. The nature of structural design and safety. Ellis Horwood; 1999.
[6] Bojadziev G, Bojadziev M. Fuzzy sets, fuzzy logic, applications. World Scientific; 1995.
[7] Bontempi F, Malerba PG, Romano L. A direct secant formulation for the R.C. and P.C. frames analysis. Studies and researches, vol. 16. School for Concrete Structures "Fratelli Pesenti", Politecnico di Milano, 1995. p. 351–86 (in Italian).
[8] Bontempi F, Malerba PG. The role of softening in the numerical analysis of R.C. framed structures. Struct Eng Mech 1997;5(6):785–801.
[9] Bontempi F, Biondini F, Malerba PG. Reliability analysis of reinforced concrete structures based on a Monte Carlo

simulation. In: Spencer Jr BF, Johnson EA, editors. Stochastic structural dynamics. Rotterdam: Balkema; 1998. p. 413–20.
[10] Brown C. A fuzzy safety measure. ASCE J Eng Mech Div 1979;105(5).
[11] CEB. Reinforced concrete elements under cyclic loading state-of-the-art report. Bull Inf 1996;230.
[12] CEB. Nonlinear analysis. Bull Inf 1997;239.
[13] Dong W, Shah HC. Vertex method for computing functions of fuzzy variables. Fuzzy Sets Syst 1987;24:65–78.
[14] Eibl J, Schmidt-Hurtienne B. General outline of a new safety format. CEB Bull Inf 1995;229:33–48.
[15] Jang JSR, Sun CT, Mizutani E. Neuro-fuzzy and soft computing, Matlab curriculum series. Prentice Hall; 1997.
[16] Lin TY. Strength of continuous prestressed concrete beams under static and repeated loads. ACI J 1955;26(10):1037–59.
[17] Malerba PG. Limit and nonlinear analysis of reinforced concrete structures. Udine, Italy: CISM International Centre for Mechanical Sciences; 1998 (in Italian).
[18] Michalewicz Z. Genetic algorithms + data structures = evolution programs. Berlin: Springer; 1992.
[19] Valliappan S, Pham TD. Fuzzy logic applied to numerical modelling of engineering problems. Comput Mech Adv 1995;2:213–81.
[20] Yao JTP, Furuta H. Probabilistic treatment of fuzzy events in civil engineering. Prob Eng Mech 1986;1(1).
[21] Zadeh LA. Fuzzy sets. Inf Control 1965;8:338–53.